Drip water isotopes in semi-arid karst

Cuthbert, Mark O.; Baker, Andy; Jex, Catherine N.; Graham, Peter W.; Treble, Pauline C.; Andersen, Martin S.; Ian Acworth, R.

DOI:
10.1016/j.epsl.2014.03.034

Drip water isotopes in semi-arid karst: implications for speleothem paleoclimatology

Mark O. Cuthbert[1, 2], Andy Baker[3,4*], Catherine N Jex[3,4] , Peter Graham[3], Pauline Treble[5], Martin S. Andersen[1,4], R. Ian Acworth[1,4]

[1]Connected Waters Initiative Research Centre, UNSW Australia, 110 King St, Manly Vale, NSW2093, Australia

[2]School of Geography, Earth and Environmental Sciences, University of Birmingham, Edgbaston, B15 2TT, UK

[3]Connected Waters Initiative Research Centre, UNSW Australia, Sydney, NSW2052

[4]Affiliated to the National Centre for Groundwater Research and Training, Australia

[6]Institute for Environmental Research, Australian Nuclear Science and Technology Organisation, New Illawarra Road, Lucas Heights, Australia, NSW 2234

*corresponding author: a.baker@unsw.edu.au

Abstract

We report the results of the first multi-year monitoring and modelling study of the isotopic composition of drip waters in a semi-arid karst terrane. High temporal resolution drip rate monitoring combined with monthly isotope drip water and rainfall sampling at Cathedral Cave, Australia, demonstrates that drip water discharge to the cave occurs irregularly, and only after occasional long duration and high volume rainfall events, where the soil moisture deficit and evapotranspiration is overcome. All drip waters have a water isotopic composition that is heavier than the weighted mean annual precipitation, some fall along the local meteoric water line, others trend towards an evaporation water line. It is hypothesised that, in addition to the initial rainfall composition, evaporation of unsaturated zone water, as well as the time between infiltration events, are the dominant processes that determine infiltration water isotopic composition. We test this hypothesis using a soil moisture balance and isotope model. Our research reports, for the first time, the potential role of sub-surface evaporation in altering drip water isotopic composition, and its implications for the interpretation of speleothem $\delta^{18}O$ records from arid and semi-arid regions.

Keywords: evaporation, water isotopes, recharge, karst, speleothems, semi-arid

1. Introduction

Within-cave monitoring of climate, hydrology and drip water biogeochemistry is recognised by the speleothem paleoclimate research community as being essential to the understanding of speleothem proxy records. Numerous monitoring studies have been reported in recent years, many of which are long-term (for example, Baker and Brunsdon, 2003; McDonald et al 2007) and include both monitoring and modelling approaches (for example, Treble et al., 2013). However, to date these research efforts have been mostly focussed on understanding processes relevant to temperate, sub-alpine and alpine caves. This bias has been predominantly due to the ease of access of cave sites, and the location of cave research groups, rather than the lack of importance of monitoring studies that would be relevant to speleothem records in semi-arid to arid climates.

The most widely used speleothem paleoclimate proxy is $\delta^{18}O$: originally sourced from precipitation, the speleothem water isotopic composition can be later modified due to interactions in the soil and vadose zones and within the cave. In semi-arid environments, the relationship between rainfall and soil water isotopic composition is relatively well understood thanks to series of field and laboratory studies (Allison 1982, Allison et al 1983, 1987; Allison and Hughes 1983; Barnes and Allison 1988). The occasional rainfall events in a semi-arid climate will infiltrate the soil, leaving an isotopic signature of the precipitation event. Subsequent evaporation leads to a soil water isotope profile that is exponential in profile and isotopically enriched towards the surface. However, as evaporation is the dominant soil hydrological process, the soil volumetric water content is low as water is lost by evaporation. Therefore, on the occasions where the soil moisture deficit is exceeded and groundwater recharge occurs, it is likely that 'old' and isotopically enriched soil water is volumetrically small compared to the event water, and therefore water infiltrating to the vadose

zone is likely to have negligible water isotopic enrichment. In contrast to the relatively well understood soil water isotope processes, there are almost no studies that have investigated water isotope processes in the vadose zone in semi-arid to arid environments. In karst systems, Ingraham et al (1990) is a lone study that investigates the water isotopic composition of pool waters in the Carlsbad cave system of New Mexico, USA, to help constrain evaporative water fluxes within the cavern.

Here we report the results of a two-year drip water and rain water isotope monitoring study from Cathedral Cave at Wellington, New South Wales, Australia. Mean annual precipitation is 619 mm (1956-2005) and evaporation is 1825 mm (1965-2005; recorded at the nearby Wellington Research Centre, Australia Bureau of Meteorology). At this site ET>>P and so the processes inferred from our monitoring of drip water isotopic composition are most relevant to semi-arid and arid climate regions. Additionally, we utilize the monitoring results to constrain a modified soil moisture balance model. Extending the approach of Cuthbert et al (2013), we add a soil and groundwater isotope component to understand the processes controlling drip water isotopic composition at our site.

2. Methods and Site Description

2. 1 Site background

Our monitoring and modeling experiment was undertaken at Cathedral Cave in Wellington, New South Wales, Australia (32 37'S; 148 56'E) (Figure 1). The cave entrance, at 325.16 m elevation, is situated close to the top of a north-south trending ridge formed from Devonian Garra Formation limestone. To the west of this ridge, at an elevation of c. 300m, are the alluvial gravels of the Bell River. The geomorphology of the cave has been extensively researched (Osborne et al 2007) and is primarily orientated along the direction of jointing (150°), and contains abundant evidence of hypogene formation processes, arguably typical of many caves in SE Australia (Osborne et al., 2010 The cave descends approximately 25m from the entrance to the end of the cave, where the cave is

flooded as it intercepts the local groundwater at The Well (Figure 1). Groundwater is observed at an elevation of between 280-300m asl, depending on antecedent climate conditions. The cave is overlain by degraded box grass woodland, with bare soil and sparse tree cover (Blyth et al., 2014).

Our observations of the cave climatology are consistent with its morphology, which is a descending dead-end cave. Two entrances, located at the same elevation in the entrance series, could lead to limited ventilation in that part of the cave. Air exchange close to the entrance would also be expected through pressure and density effects on both the cave air and groundwater level. Air temperature measurements using Star-Oddi micro loggers show little variation (18.25±0.05°C, August 2011 to August 2012) in South Passage (our Site 2, Figure 1) over the long-term. Near the entrance (site 1, Figure 1), we have logged temperature variability over the short term and observe a range of 17-18 °C in January 2013 and 18-23 °C in February 2014. Relative humidity in the cave has been recorded using a Campbell HMP155A over short campaigns and was observed to be constant at 97% at Site 2 (Jan-Feb 2014), consistent with the presence of an adjacent groundwater body, and variable from 73-93% at site 1, consistent with ventilation within the entrance series. Within cave evaporation has been measured by measuring the volumetric water loss of 50ml water placed in petri dishes: at Site 1, average evaporation was 0.14 mm/d (over the period 7-15 January 2014) and 0.08 mm/d (15 January - 6 March 2014) and at Site 2 was 0.004 mm/d (15 January – 6 March 2014).

The cave has been a focus of long-term hydrogeological monitoring by the investigators, commencing in 2009 and continuing, primarily using a network of in-situ Stalagmate © drip loggers. Jex et al (2012) describe drip water patterns and processes within the cave for a spatially dense network of drip-collection sites: it is a subset of drip waters from this network at Site 2 which are investigated here. Mariethoz et al (2012) utilized near-surface infiltration to identify non-linear and chaotic drip behavior and its relationship to surface connectivity. Most recently, and subsequent to

106 the results presented here, at Site 1, we have undertaken an artificial irrigation experiment to better
107 understand infiltration processes (Cuthbert et al., in review; Rutlidge et al., in revison).
108
109 *2. 2 Monitoring methods*
110 Our water isotope monitoring program was designed as follows. Monthly integrated rainfall samples
111 were collected using standard IAEA protocols (http://www-naweb.iaea.org/
112 napc/ih/documents/userupdate/sampling.pdf) at the nearby (7 km) UNSW Wellington Field Station.
113 Drip water was collected at fifteen monitoring sites within the South Passage of Cathedral Cave (Site
114 2, Figure 1); five (sites 279, 280, 372, 395 and 396) were part of the network described by Jex et al.
115 (2012). Isotope water samples were collected via funnels connected to 500ml or 1l HDPE bottles.
116 Paraffin was placed in the bottles as a precaution to prevent evaporation within the bottles.
117 Evaporation could be possible anywhere prior to collection, although our within-cave relative
118 humidity measurements suggest that this is unlikely to occur within the cave at Site 2. Bottles were
119 changed monthly, with fresh paraffin added, and an integrated 30 ml water sample transferred to
120 sealed glass McCartney bottles with no headspace to prevent evaporation whilst in storage. These
121 bottles were then stored until analysis, which occurred within two months. Water samples were
122 collected at monthly intervals from March 2011 to March 2013.
123
124 Drip rates were monitored using a network of twenty-six Stalagmate © drip loggers in South Passage
125 (Site 2) and a further four drip loggers situated closer to the surface (Site 1, including site 326 of Jex
126 et al., 2012). This is the expanded network referred to by Jex et al (2012). Our intention was to
127 measure the infiltration rate using Stalagmate © drip loggers for all isotope sample sites, but our
128 monthly sampling frequently disturbed the drip logger alignment, and only seven of our fifteen
129 isotope sample sites had reliable drip data. Drip rate data are presented in Table 1, together with a
130 classification of the drip type (soda straw stalactite; non-soda straw stalactite, non-soda straw
131 stalactite underneath flowstone).

Water isotopic composition of drip water and rainwater samples was determined using an LGR-24 d off-axis, integrated cavity output, cavity ringdown mass spectrometer (ICOS CRMS, Lis et al., 2007, Wassenaar et al 2008) at the University of New South Wales. Five internal reference standards (LGR#1 to LGR#5, with $\delta^{18}O$ values of -19.5‰, -16.14‰, -13.1‰, -7.69‰, -2.8‰) and one external reference standard (VSMOW2, 0‰) was analysed as an external standard; and during the analysis period we participated in the 4th IAEA Inter Laboratory Comparison for stable isotopes of water (WICO2011, laboratory 082). Two samples analysed were outside the range of the $\delta^{18}O$ standards, but by less than the analytical precision. Analytical precision for $\delta^{18}O$ was 0.17 per mil for $\delta^{18}O$ and 0.6 per mil for $\delta^{2}H$ (1σ; calculated from within run internal references materials).

2. 3 Modelling methods

A model was developed to simulate groundwater recharge, shallow karst flow and isotopic composition of drip waters at the field-site and is illustrated schematically in Figure 2. A soil moisture balance (SMB) model was used for the topsoil which, based on Cuthbert et al (2013), makes use of a combined crop co-efficient approach (K_c) taken from Allen et al. (1998). The total available water (*TAW*) in the soil is defined as:

$$TAW = (\vartheta_{FC}-\vartheta_{WP}).Z_r.(1-B) + (\vartheta_{FC}-0.5\vartheta_{WP}).Z_e.B \quad (1)$$

where ϑ_{FC} & ϑ_{WP} are fractional soil moisture contents at field capacity (FC) and wilting point (WP), Z_r is the rooting depth of crop, Z_e is the thickness of the soil layer subject to drying by evaporation, B = fractional area of bare soil (i.e. crop absent). The readily available water (*RAW*) is defined as:

$$RAW = p.TAW \quad (2)$$

where p is a factor normally between 0.2 and 0.7 (Allen et al 1998, Table 22). If the soil moisture deficit in the topsoil (SMD_s) is greater than the *RAW* then the actual evaporation rate (*AE*) is reduced using a stress co-efficient (K_s) as follows:

$$AE = K_s PE \quad (3)$$

158 $K_s = (TAW-SMD_s)/(TAW-RAW)$ (4)

159 where potential evapotranspiration, $PE = K_c PE_0$ and PE_0 is the reference crop (grass) potential
160 evapotranspiration rate.

161

162 Using a daily input time series for rates of rainfall (*RF*) and PE_0, the model algorithms calculate time
163 series of *AE* and the rate of groundwater recharge (*Rch*). Overland flow is very rare at the field site
164 and has therefore been assumed to be zero with all rainfall (*RF*) becoming infiltration. On days
165 where the soil is under stress and rainfall occurs that is less than *PE* the rainfall is transpired plus a
166 further amount from the soil equal to the remaining evaporative demand modified by the stress co-
167 efficient. If rainfall exceeds the *PE* then the excess reduces the *SMD* and once this has become zero
168 any additional excess becomes groundwater recharge.

169

170 Continuous time-series of potential evapotranspiration (PE_0) and rainfall were obtained from nearby
171 continuous automatic weather stations at the caves (Hill Station, operational from November 2011)
172 and UNSW Research Station (operational until damaged by bushfire in December 2012) and the daily
173 Bureau of Meteorology (BOM) station in Wellington (Station Number: 65034, located at Wellington
174 Agrowplow (lat: 32.56° S / Long: 148.95 °E / 350 m asl), 6.5 km from the caves). For the rainfall data,
175 double mass plots were derived for the three site combinations and the linear correlations used to
176 infill missing data from the Hill Station. PE_0 was calculated using the Penman-Montieth reference
177 crop evapotranspiration using the UNSW Research Station data and a pan factor was derived from
178 the BOM Station using a linear relationship between the two. Where data gaps persisted, the
179 correlation between average monthly temperature and average monthly PE_0 was used for filling
180 data gaps.

181

182 To estimate the drip water $\delta^{18}O$ composition reaching the cave monitoring points, rainfall events
183 were assigned isotopic compositions based on the measured monthly values and the soil store was

assumed to be fully mixed. The soil store (S1) evolved through time (*t,* in increments of Δt =1 day) according to the following mass balance equation:

$$S1_{t+\Delta t} = S1_t + (RF_t - AE_t - Rch_t).\Delta t \quad (5)$$

where $S1_t$ and $S1_{t+\Delta t}$ is the amount of water in the soil store (S1) in mm at times *t* and *t+Δt* respectively. Using the suffix δ to represent $\delta^{18}O$ isotope compositions (per mil), the soil store isotopic composition was governed by the following equation:

$$S1\delta_{t+\Delta t} = (S1\delta_t.(S1_t - (AE_t + Rch_t).\Delta t) + RF\delta_t.RF_t\,\Delta t)/S1_{t+\Delta t} \quad (6)$$

where $S1\delta_{t+\Delta t}$ and $S1\delta_t$. are the isotopic compositions of the soil store (S1) at time *t* and *t+Δt* respectively and $RF\delta_t$.is the isotopic composition of the rainfall at time *t*.

The model does not include isotopic fractionation in the soil zone for two reasons. First, at our site, recharge is erratic and comes from infrequent, large events, typical of arid and semi-arid environments. The soil is typically relatively dry before a recharge event, and even though prior soil water is likely to be enriched in heavy isotopes (Barnes and Allison, 1988), it is volumetrically very small compared to event water. Thus, during an event the residual isotopically enriched water is greatly diluted, the resulting soil isotopic concentration is very close to that of the incoming meteoric precipitation andthis prior soil water cannot be used as a tracer of water movement (Sonntag et al, 1985). A second reason for not including fractionation in the soil zone in the model is that our field data (see section 3.2) shows that the predominant fractionation process occurs under high humidity. This cannot be accounted for by in-soil evaporation processes in unsaturated soils, where near surface evaporation results in fractionation with the slope of the δD-$\delta^{18}O$ relationship typically <4 (Allison et al., 1983; Barnes and Allison, 1988).

The attenuation and isotopic evolution of the groundwater chemistry due to evaporation was then modelled by using a second store (*S2*, *S2δ* with initial values $S2_0$ and $S2\delta_0$ respectively). This filled from above with water leaving the soil as groundwater recharge, lost mass due to evaporation which

was assigned a constant value, and drained exponentially using a recession constant (τ) to simulate drip water volume and $\delta^{18}O$ to the deeper karst system (*Dr*, *Drδ*) as follows:

$$S2_{t+\Delta t} = S2_t + (Rch_t - E - Dr_t).\Delta t \quad (7)$$

with $Dr_t = \tau.S2_t$ (8)

The isotopic composition of the karst store (and any water leaving the store to become drip water) was assumed to be governed by a simple mass balance if the depth of water in the store was greater than a threshold value ($S2_{lim}$):

$$S2\delta_{t+\Delta t} = (S2\delta_t.(S2_t - (Dr_t+E).\Delta t) + S1\delta_t.Rch_t.\Delta t)/S2_{t+\Delta t} \quad (9)$$

However, if $S2_t<S2_{lim}$ then it was assumed, following Gonfiantini (1986, Eq.7, p117), that an evaporative process in the shallow karst was of the form as follows:

$$S2\delta_{t+\Delta t} = (S2\delta_t - m).f^n + m \quad (10)$$

Where *m* and *n* are empirical constants to be determined from model calibration, and *f* is the proportion of water left in the store since the level fell below the threshold amount.

Rather than producing a calibrated model for each drip site with different parameters, our approach was rather to attempt to match the range of observed isotopic values with the purpose of testing our conceptual model and providing estimates of the range of model parameter combinations. The SMB flow model was first tuned to capture the overall timing of the main drip events monitored in South Passage by varying the SMB parameters; it was not attempted to match the volume of drip water leaving the karst store against the measured drip data since the distribution of recharge through the karst network is extremely complex and highly variable across all drip sites. This stage of the model refinement was carried out manually since no single objective function could reasonably be defined against which to automate the calibration. For the estimation of parameters for the isotope model we applied a method similar to the widely used GLUE methodology (Beven & Binley 1992) as follows. The aggregated modelled monthly drip water composition was compared directly against the range of measured values assuming drip water is all sourced from a single

shallow store (albeit at different rates) by varying the parameters controlling the karst store and fractionation process. Sets of prior parameter distributions (ranges of estimated initial values) were defined based on physical plausibility and initial experimentation with the model to ensure a wide enough spread to avoid unwanted rejection of any physically plausible parameter sets. Monte-Carlo simulations were carried out for 50 000 random combinations of the prior parameter distributions. If all modelled values fitted within the range of the measured isotopic composition of the drip water across all samples for a given time step this model was deemed 'behavioural' and these models were retained (henceforth: physically plausible models). The parameter values of these physically plausible models were used to define the posterior parameter distributions..

3. Results and Discussion

3.1 Rainfall, evapotranspiration, and drip rates

Rainfall, calculated PE_0 and drip water data for the two-year period are presented in Figure 3. Average rainfall and PE_0 for Feb 2011 to Feb 2013 are 666 and 982 mm/yr, higher and lower than the long term average respectively, reflecting the slightly cooler and wetter conditions experienced during the monitoring period where La Nina or neutral conditions prevailed. Drip rates are observed to be highly episodic, with only a few rainfall events of high duration and amount resulting in recharge and thus exfiltration in the cave. Drip water responses within the cave show significant variability between sites, as previously demonstrated by Jex et al. (2012). Particularly large drip rates, sometimes over 100 drips per 15 minutes (equivalent to ~$1x10^{-5}$ l s^{-1}), were observed during Jan-Mar 2012 and Jul-Aug 2012 with periods in between of much slower exfiltration ranging from 0 to approx. 10 drips per 15 minutes (<~$1x10^{-6}$ l s^{-1}).

3. 2 Water Isotopes

The $\delta^{18}O$ and $\delta^{2}H$ composition of monthly integrated drip water and rainfall samples are summarized in Table 1, and $\delta^{18}O$ time-series plotted in Figure 3. Figure 4 presents the plot of $\delta^{2}H$ vs. $\delta^{18}O$: also

261 presented on this plot are monthly grab samples collected from adjacent rivers (open squares) and
262 ground water (open circles). River samples were obtained from the Macquarie River at the UNSW
263 Research Station (7 km to the north-east of the caves) and the Bell River (2 km downstream of the
264 Wellington Caves). Ground water samples were collected within the Wellington Caves Reserve, from
265 Anticline Cave (200 m west of the cave entrance) and from 'The Well' in Cathedral Cave (shown in
266 Figure 1).
267
268 Figure 4 demonstrates that the monthly rainfall samples fall along a local meteoric water line
269 (LMWL) with an equation $\delta^2H = 7.29\ \delta^{18}O + 7.68$ (r=0.96, standard error of the slope = 0.43, standard
270 error on the intercept = 2.08). The annual weighted mean isotopic composition of rainfall over the
271 monitoring period was -4.28‰ for $\delta^{18}O$ and -23.54‰ for δ^2H, and the river and ground water grab
272 samples all had a mean isotopic composition that reflected the weighted mean of precipitation
273 (Table 1). In contrast, the drip water mean $\delta^{18}O$ and δ^2H composition ranged from -1.51‰ to -
274 3.45‰, and -1.16‰ to -17.72‰, respectively. Mean drip water isotopic compositions were
275 therefore 0.83 to 2.77‰ ($\delta^{18}O$) and 5.82 to 22.38‰ (δ^2H) heavier than the weighted mean annual
276 precipitation.
277
278 We observe no relationship between drip water isotopic composition and hydrological properties
279 such as the drip source classification, or drip rate (at the sites where that data is available) (Table 1).
280 Comparing drip source classifications to drip water oxygen isotopic composition, soda-straw (n=8)
281 and non-soda straw (n=5) stalactite drip sources have mean isotopic compositions that are
282 statistically similar (students t-test, 95% confidence level). Comparing mean, mean and maximum
283 drip rates to oxygen isotopic composition, for the drip sites where data is available (n=7), gave slopes
284 of the $\delta^{18}O$ vs drip rate relationship not significantly different from zero
285

Typically, from a theoretical perspective, the presence of a water isotopic composition that is heavier than the weighted mean of precipitation would be expected to be due to evaporation of lighter isotopes. The relative enrichment of δ^2H to $\delta^{18}O$ varies with the processes that determine evaporative enrichment: the relative humidity and turbulence of the overlying air mass (Gonfiantini, 1986). In environments with limited air movement, the relative humidity can approach 100%; the slope of the δ^2H vs. $\delta^{18}O$ regression will increase and the maximum amount of enrichment decreases with increasing relative humidity. Following Gonfiantini (1986), in environments with relative humidity larger than 95% the slope of the δ^2H vs. $\delta^{18}O$ regression will be similar to that of the LMWL with an enrichment of up to 4‰ in $\delta^{18}O$ possible. In environments with a lower humidity, the slope of the δ^2H vs. $\delta^{18}O$ regression decreases, and the maximum amount of enrichment will be greater. Applying this theory to our results, Figure 4 demonstrates that drip waters as a whole scatter along the LMWL. However, considering each drip site individually, some sites have a slope of the δ^2H vs. $\delta^{18}O$ regression that is, within the standard error uncertainty (Table 1), the same as the slope of the δ^2H vs. $\delta^{18}O$ regression of the LMWL, indicative of evaporation in a high humidity environment. Others which have a lower slope of the δ^2H vs. $\delta^{18}O$ regression than the LMWL, which could be attributed to evaporative enrichment in a less humid environment. Individual regression data is presented in Table 1.

In order to investigate these data further, Figure 5 presents the $\delta^{18}O$ isotopic composition against time for drip sites grouped by their slopes of the δ^2H vs. $\delta^{18}O$ regression. Sites which have a similar δ^2H vs. $\delta^{18}O$ slope to the LMWL (slope of the δ^2H vs. $\delta^{18}O$ regression >6.8; sites 279, 280, 320, 372, 387 and 398) have very similar time series. It is also notable that there is no relationship between the rainfall isotopic composition (Figure 3) and the way drip water isotopes vary during periods of no recharge. Sites which have the lowest slopes of δ^2H vs. $\delta^{18}O$ (slope of the δ^2H vs. $\delta^{18}O$ regression <4.8; sites 319, 322, 330, 380, 396) also have similar time series. However, this group has greater isotopic variability between sites, with some having a wider range towards heavier isotopic

compositions. Notably, when comparing the slope of individual δ^2H vs. $\delta^{18}O$ regressions vs. mean isotopic composition, no relationship was observed, but a strong correlation is present between the slope of the δ^2H vs. $\delta^{18}O$ regression and its correlation coefficient (r=0.92). Sites with a steeper slope (e.g. that fall on the LMWL) have the strongest correlation between δ^2H vs. $\delta^{18}O$; sites with a lower slope have the weakest correlation between δ^2H vs. $\delta^{18}O$.

Inspection of Figures 4 and 5 demonstrates that the drip sites can be interpreted in the following way:

Type 1. Some sites have variable $\delta^{18}O$, δ^2H vs. $\delta^{18}O$ slopes >6.8 and similar to the LMWL, and very similar time-series. Some sites have discontinuous dripping, with drip flow commencing after the high rainfall events, and the isotopic composition of this initial drip water varies between events. The isotopic composition of the water subsequently becomes heavier during drip flow recession periods. A conventional explanation would be that the drip water comes from a single water source. Isotopic enrichment must occur in this source, and the δ^2H vs. $\delta^{18}O$ slope demonstrates that if evaporation is the explanation for the enrichment, it must occur in a humid (>95% relative humidity) environment (Gonfiantini, 1986). Sites with slopes of the δ^2H vs. $\delta^{18}O$ regression >6.8 are distinguished in Figure 5. Figure 6 demonstrates that they show a spatial clustering, with no relationship to drip classification (Table 1)..

Type 2. Some sites have variable $\delta^{18}O$, δ^2H vs. $\delta^{18}O$ slopes <6.8 and lower than the LMWL, and more variability between the time-series. Similar to sites with slopes of the δ^2H vs. $\delta^{18}O$ regression >6.8, drip flow can be continuous or discontinuous and shows large variations when recharge occurs. Drip sites have an isotopic composition of the water which subsequently becomes heavier, even during periods of drip flow recession, with greater variability and enrichment of $\delta^{18}O$ than sites with slopes of the δ^2H vs. $\delta^{18}O$ regression >6.8. Sites are distinguished by their slope (5.8-6.8, 4.8-3.8, and <3.8) in Figure 5 and spatial distribution in Figure 6.

Type 3. One site has a low variability of $\delta^{18}O$ and a mean composition that is heavier than the weighted mean of precipitation. It can be hypothesized that these sites have a relatively homogenized water source that has undergone isotopic enrichment. Only one such sample is present in our monitoring network, Site 319 (Figure 5, 6).

Combined isotope and drip rate data demonstrate that the drip water isotopic composition can be explained by the following processes:

1) A flow path where the resultant drip water has an initial isotopic composition that reflects the previous infiltration event, and which becomes increasingly isotopically heavy over time but falls on the LMWL. We hypothesise that this is water stored within the shallow unsaturated zone in which evaporation occurs, as observed in laboratory environments (e.g. Ingraham and Criss, 1993). The evaporation has to occur in an environment where RH>95%, which enriches the isotopic composition close to the LMWL (Gonfiantini, 1986). For this to occur, the store has to be near-surface, to experience diurnal temperature changes necessary for continued evaporation. While allowing sufficient vapour transport to keep driving the evaporative process, it must also be relatively enclosed to permit continual drainage of evaporated (increasingly enriched) water whilst maintaining a high humidity. Although previously unreported as an isotopic process in karst, such a mechanism is possible in hot continental climates which experience large diurnal temperature variations; soil temperature variations lagged from the atmospheric temperature variations could drive circulation of air in and out of the soil/karst voids. The spatial clustering of these sites (slopes of the $\delta^{2}H$ vs. $\delta^{18}O$ regression larger than 6.8 in Figure 6) suggests discrete water stores where evaporation is occurring.
2) A flow path similar to (1) above, but where water also experiences evaporative enrichment at lower relative humidity. For this to occur, the air-filled part of the store could be larger, or

better ventilated, or the enrichment could occur within a subsequent cave void if infiltration rates are low and relative humidity low. These sites are have slopes of the δ^2H vs. $\delta^{18}O$ regression of <6.8 in Figure 4.

Most infiltration sites comprise a mixture of these two end-member scenarios. For all drip sites combined, the slope correlates with the individual drip water isotope δ^2H vs. $\delta^{18}O$ correlation (r=0.92), as noted previously. The strong association between the slope of the δ^2H vs. $\delta^{18}O$ regression at a drip site and the strength of correlation between δ^2H vs. $\delta^{18}O$ (Table 1) suggests that the single, RH>95% evaporation end-member is the primary source of fractionation, with some drips experiencing additional fractionation at lower RH.

3.3 Modelled flow and water isotopes

Figures 3 and 7 show the modelled karst potential groundwater recharge flux indicating that the combined SMB-karst model captures the timing of the main drip water events well. Calibrated model parameters are shown in Table 2.

The model is able also to simulate the observed patterns and magnitudes of the drip water isotopic composition using the parameters given in Table 2 and Figure 5. The set of physically plausible models, despite being 'free' to vary within the entire range of observable drip composition for Types 1 to 3 identified above, included no models which consistently maintained $\delta^{18}O$ values as low as Site 319, of Type 3. This suggests that the 'single karst store' model structure works well for Types 1 and 2 thus supporting our conceptual model. For Type 3, a mixed source of water is needed, derived from more than one store and so to successfully simulate such siteswould require a modification of the existing numerical model to a more complex model structure.

If the karst evaporative process is 'switched off' (Figure 7) the modeled isotopic drip water reverts to lighter values which vary little from the mean rainwater isotopic composition. This shows that the observed drip water isotopic variations cannot simply be explained by transformation of the input precipitation signal using a standard model of soil and shallow karst processes. It is thus strongly indicative of evaporative equilibrium fractionation (i.e. at conditions >95% RH) in the karst being the dominant mechanism controlling the observed isotopic drip water compositions. Although the evaporative process is modeled empirically it has a sound theoretical basis with Equation 10 being of the form suggested by Gonfiantini (1986, Eq.7, p117). In the present case the variable *f* changes not only due to evaporative loss but also due to drainage from the karst store. Hence, a direct comparison between our parameters *n* and *m*, and Gonfiantini's *A* and *B* parameters cannot be made without further (laboratory) investigation to determine the precise form this relationship should take. The values of the physically based parameters retained in the posterior set are physically plausible and lend insight into the potential properties of the karst unsaturated zone at the fieldsite. Most parameters have clearly defined optima for example $\tau \approx 0.03$ /d, $S2_{lim} \approx 60$ mm and $S2_0 \approx 200$ mm. The relatively large initial value for $S2_0$ is suggestive of a period of substantial recharge occurring just prior to the drip isotope monitoring period. This is consistent with high observed driprates from the site in late 2010, observed prior to cave flooding (Jex et al., 2012). Furthermore, the ranges of *S2* and the drainage function, τ, are also reasonable in comparison to other karst models (for example, Bradley et al., 2010). The model is relatively insensitive to the evaporation flux (which was set to a maximum of 0.15 mm/d, constrained by our in-cave evaporation rate at Site 1) in determining the timing of the positive isotopic value excursions since the optimum $S2_{lim}$ values are relatively large in comparison. Hence the isotopic composition is primarily controlled by the empirical *m* and *n* parameters which control the fractionation of the karst store as it loses water by drainage and evaporation and which have very clearly defined parameter optima at $n \approx 0.3$, $m \approx -2$,.

The way the model is structured, the rate of fractionation is explicitly dependent on the fraction of water remaining in a shallow karst store. However, since the modeled drip rates are directly proportional to the size of this store (via the recession constant), the fractionation is thus also proportional to the drip rate, below a threshold value. Such a flow rate-dependent evaporative process has recently been directly observed during film flow over a speleothem-forming feature in the shallower part of the Cathedral Cave system (Cuthbert et al., in review). This could also be responsible for the fractionation observed in the deeper South Passage samples reported here. Furthermore, additional evaporative fractionation could occur within the cave passage, especially at low drip rates, either on the stalactite or on the sample collection bottle prior to collection below the paraffin seal (Dreybrodt and Deininger, 2013). However, the high relative humidity in South Passage, and lack of observed relationship between drip rate, drip classification and oxygen isotopic composition, suggests that these effects would be limited, at least at site 2.

It is notable that the recharge events which reset the isotopic composition of the karst store and drip waters in South Passage occur on timescales of hours to days and time-steps of this order of magnitude are needed to predict their occurrence. It is well known that soil moisture balance models are very sensitive to the choice of time-stepping (Howard & Lloyd 1979). However, most climate models operate on monthly or coarser time-steps and, when coupled with hydrologic models, structural errors such as those due to time-stepping within a soil-moisture accounting algorithm are rarely considered (Holman et al., 2012). Our results therefore have significant implications for how to model adequately the effect of climate change, for example variations in rainfall intensification, on recharge and speleothem-forming processes in karst environments.

3.4 Implications for speleothem records

Our results inform the climatic interpretation of speleothem records in the arid and semi-arid environment in Australia and elsewhere. We have shown that drip water may be enriched by several per mil owing to evaporative processes; this is of similar magnitude, but opposite in direction, to the

441 fractionation predicted by the estimated atmospheric cooling of up to 9 °C at the Last Glacial
442 Maximum in continental Australia (Galloway, 1965; Miller et al., 1997). Thus if both processes are
443 happening concurrently the speleothem signal could be confounded and affect the imprint of
444 atmospheric temperature in the speleothem record (Fairchild and Baker, 2012). Additionally, we
445 expect that the speleothem isotopic record from these environments may exhibit a considerable
446 range in isotopic values driven by shifts in the frequency-magnitude relationships of infiltration
447 events. This may be recorded on an event-scale but, more relevant to the detection in speleothem
448 isotopic records, is the decadal-centennial timescale on which recharge will be influenced by
449 variability in the dominant climate modes over Australia and more generally in other semi-arid and
450 arid areas globally. Variability in climate modes on these timescales has been observed in proxy
451 records in the Australisian region (e.g. van Ommen et al., 2010). Finally, we draw a link between
452 these results and previous studies that have demonstrated a sensitivity between the timing of
453 speleothem growth and the P-ET balance. Speleothems 'switching on' during cooler time periods
454 (the Last Glacial Maximum and stadial periods) is attributed to reduced evaporation in southern
455 Australia's arid margin (Ayliffe et al., 1998; Cohen et al., 2011). The results of our study may inform
456 the interpretation of speleothem isotopic records from this region as the water balance changes
457 within stadial and glacial events.
458
459 **Conclusions**
460 Groundwater recharge in semi-arid environments is episodic; the initial isotopic composition of
461 recharge reflects the isotopic composition of the few rainfall events which are large enough to
462 overcome existing soil moisture deficits. This initial isotopic composition may be affected by
463 subsequent evaporation. At our monitoring site, observed drip waters had a mean $\delta^{18}O$ up to 2.77‰
464 heavier than the weighted mean of precipitation. Here, evaporation from a partially air-filled water
465 store in a high humidity environment is an important process. Our modelling approach
466 demonstrated that this isotope enrichment had to include evaporation from a shallow subsurface

467 karst water store, such as a solutionally widened fracture or proto-cave. The degree of enrichment
468 would be site specific, and dependent on the relative size of the store and its climatic properties
469 (temperature variability, relative humidity), its drainage rate and the time between infiltration
470 events. We have identified and modelled unsaturated zone evaporation as an important process in
471 determining infiltration water $\delta^{18}O$ for the first time. We propose that at other caves in semi-arid to
472 arid regions, evaporation will also be a likely source of isotope enrichment, but this requires
473 confirmation.
474
475 At Cathedral Cave, infiltration $\delta^{18}O$ is a complex function of (1) the isotopic composition of recharge
476 water, (2) the time since the last recharge event (3) water store climate and physical properties and
477 (4) water flow routing from the store to the drip site, including evaporation during the degassing
478 process that forms speleothems (Dreybrodt and Deininger, 2013). This makes the interpretation of
479 individual stalagmite $\delta^{18}O$ records potentially complex. The range of mean drip water $\delta^{18}O$ between
480 sample sites gives an indication of this hydrological uncertainty: in our case this is 1.94‰ (mean
481 from -1.51‰ to -3.45‰). This is greater than the total range of hydrological uncertainty in
482 stalagmite $\delta^{18}O$ currently modelled for both modern (Baker and Bradley, 2009; Bradley et al. 2010;
483 Treble et al. 2013), historical (Jex et al. 2013), and Last Glacial Maximum (Baker et al. 2013)
484 environments: all use hydrology modelling approaches that exclude unsaturated zone evaporation
485 as a process.
486
487 Interpretation of speleothem $\delta^{18}O$ archives, typically from temperate, sub-alpine or cool climates, is
488 one where evidence is presented either (1) for speleothem deposition that is at or close to
489 equilibrium, or (2) that deposition has occurred out of equilibrium, such that kinetic fractionation
490 has occurred (Fairchild and Baker, 2012). The relevant processes in these environments are relatively
491 well observed (e.g. Spötl et al., 2005; Lachniet, 2009) and modelled (Dreybrodt and Scholz, 2011).
492 However, in semi-arid to arid environments, subject to surface, soil and unsaturated zone

493 evaporation, our understanding of the interpretation of speleothem $\delta^{18}O$ is still developing. In this
494 study, we attribute at least part of the observed $\delta^{18}O$ isotope composition of stalagmite forming drip
495 waters to evaporation in the unsaturated zone, and propose that this process is likely to occur at
496 other sites where ET>P, such as those reported in central Texas (Pape et al., 2010). Thus,
497 interpretation of stalagmite $\delta^{18}O$ in these regions could be a function of this process, as well as the
498 previously recognised within-cave processes such as kinetic effects (due to the differing rate
499 constants of calcite precipitation for the heavy and light isotopes; Dreybrodt, 2008; Dreybrodt and
500 Scholz, 2011) and evaporation during degassing (Dreybrodt and Deininger, 2013). As well as having
501 relevance to the interpretation of speleothem records from modern day regions where ET>P and
502 infiltration is infrequent, our findings are also relevant to the interpretation of Quaternary
503 speleothem records from regions where the modern day climate is temperate or Mediterranean, but
504 in the past experienced some degree of aridity.
505
506 **Supplementary Materials**
507 Rainfall double mass plots, isotope and drip rate data are available on-line as supplementary
508 spreadsheets.
509
510 **Acknowledgements**
511 CJ, AB, MSA and RIA were supported the NCGRT, PG by the NSW Science Leveraging Fund and MOC
512 by the European Community's Seventh Framework Programme [FP7/2007-2013] under grant
513 agreement n°299091. Groundwater infrastructure used by the research team was funded by the
514 Australian Government Groundwater Education Investment Fund and weather station data
515 downloaded from (http://groundwater.anu.edu.au). We thank Monika Markowska for provision of
516 South Passage temperature data and Even Jensen and Gabriel Rau for provision of relative humidity
517 data, Wellington Council for permission to work at the Wellington Caves site, and Chris George, Col

518 Birchall, Mike Augee and staffe at Wellington Caves that made this research possible. The reviews of
519 Darrel Tremaine and two anonymous reviewers greatly improved the clarity of the manuscript.
520

521 **References**

522 Allison, G.B., 1982. The relationship between ^{18}O and deuterium in water in sand columns
523 undergoing evaporation. Journal of Hydrology, 55, 163-169.

524 Allison, G.B. and Hughes, M.W., 1983. The use of natural tracers as indicators of soil-water
525 movement in a temperate semi-arid region. Journal of Hydrology, 60, 157-173

526 Allison, G.B., Barnes, C.J. and Hughes, M.W., 1983. The distribution of deuterium and 18O in dry
527 soils. 2. Experimental. Journal of Hydrology, 64, 377-397.

528 Allison, G.B., Colin-Kaczala, C., Filly, A. and Fontes, J.Ch. 1987. Measurement of isotopic equilibrium
529 between water, water vapour and soil CO_2 in arid zone soils. Journal of Hydrology, 95, 131-141

530 Allen, R.G., Pereira, L.S., Raes, D., and Smith, M. 1998. Crop evapotranspiration - Guidelines for
531 computing crop water requirements - FAO Irrigation and drainage paper 56. FAO, Rome, Italy.

532 Ayliffe, L.K., Marianelli, P.C., Moriarty, K.C., Wells, R.T., McCulloch, M.T., Mortimer, G.E. and
533 Hellstrom, J.C., 1998. 500ka precipitation record from southeastern Australia: Evidence for
534 interglacial relative aridity. Geology 26, 147-150.

535 Baker, A. and Brunsdon, C., 2003. Non-linearities in drip water hydrology: an example from Stump
536 Cross Caverns, Yorkshire. Journal of Hydrology, 277, 151-163.

537 Baker, A. and Bradley, C. 2010. Modern stalagmite $\delta^{18}O$: instrumental calibration and forward
538 modelling. Global and Planetary Change, 71, 201-206.

539 Baker, A., Bradley, C. and Phipps, S.J., 2013. Hydrological modelling of stalagmite $\delta^{18}O$ response to
540 glacial-interglacial transitions. Geophysical Research Letters. 40, Issue 12, 3207–3212

541 Barnes, C.J. and Allison, G.B., 1988. Tracing of water movement in the unsaturated zone using stable
542 isotope of hydrogen and oxygen. Journal of Hydrology, 100, 143-176.

543 Beven, K., and Binley, A., 1992. The future of distributed models: model calibration and uncertainty

544 prediction. Hydrological processes, 6, 279-298.

545 Bradley, C., Baker, A., Jex, C. and Leng, M.J. 2010. Hydrological uncertainties in the modelling of cave
546 drip-water $\delta^{18}O$ and the implications for stalagmite palaeoclimate reconstructions. Quaternary
547 Science Reviews 29, 2201-2214.

548 Cohen, T.J., Nanson, G.C., Jansen, J.D., Jones, B.G., Jacobs, Z., Treble, P., Price, D.M., May, J.H., Smith,
549 A.M., Ayliffe, L.K., and Hellstrom, J.C., 2011. Continental aridification and the vanishing of Australia's
550 megalakes. Geology 39, 167-170.

551 Cuthbert, M.O., Mackay, R. and Nimmo, J.R. 2013. Linking soil moisture balance and source-
552 responsive models to estimate diffuse and preferential components of groundwater recharge.
553 Hydrology and Earth System Science, 17, 1003-1019.

554 Cuthbert, M.O., Rau, G.C., Andersen, M.S., Roshan, H., Rutlidge, H., Marjo, C., Markowska, M.,
555 Graham, P.W., Mariethoz, G. and Baker, A., in review. Controls on cave dripwater temperatures and
556 implications for speleothem paleoclimate archives. Geophysical Research Letters.

557 Dreybrodt, W. 2008. Evolution of the isotopic composition of carbon and oxygen in a calcite
558 precipitating H_2O-CO_2-$CaCO_3$ solution and the related isotopic composition of calcite in stalagmites.
559 Geochimica et Cosmochimica Acta, 72, 4712-4724.

560 Dreybrodt, W. and Scholz, D. 2011. Climatic dependence of stable carbon and oxygen isotope signals
561 recorded in speleothems: From soil water to speleothem calcite. Geochimica et Cosmochimica Acta,
562 75, 734-752

563 Dreybrodt, W. and Deininger, M., 2013. The impact of evaporation to the isotope composition of DIC
564 in calcite precipitating water films in equilibrium and kinetic fractionation models. Geochimica et
565 Cosmochimica Acta, doi 10.1016/j.gca.2013.10.004

566 Fairchild, I.J. and Baker, A., 2012. Speleothem Science. Wiley-Blackwell.

567 Galloway, R.W., 1965. Late Quaternary climates in Australia. Journal of Geology 73, 603-618.

568 Gonfiantini, R., 1986. Environmental Isotopes in Lake Studies. In Fritz P. and Fontes J. Ch. (Eds)
569 Handbook of Environmental Isotope Geochemistry, Volume 2: The Terrestrial Environment, pp113-
570 168. Elsevier.
571 Holman I. P., Allen, D. M., Cuthbert M. O. and Goderniaux P. 2012. Towards best practice for
572 assessing the impacts of climate change on groundwater. Hydrogeology Journal, 20: 1-4.
573 Howard, K. W. F., and Lloyd, J. W. 1979. The sensitivity of parameters in the Penman evaporation
574 equations and direct recharge balance. Journal of Hydrology, 41(3), 329-344.
575 Ingraham, N.L., Chapman, J.B. and Hess, J.W., 1990. Stable isotopes in cave pool systems: Carlsbad
576 Cavern, New Mexico, U.S.A. Chemical Geology, 86, 65-74.
577 Ingraham, N.L. and Criss, R.E., 1993. Effect of surface area and volume on the rate of isotopic
578 exchange between water and water vapour. Journal of Geophysical Research, 98, D11, 20547-20553.
579 Jex, C.N., Mariethoz, G., Baker, A., Graham, P., Andersen, M.S., Acworth, I., Edwards, N. and Azcurra,
580 C., 2012. Spatially dense drip hydrological monitoring and infiltration behaviour at the Wellington
581 Caves, South East Australia. Int Journal of Speleology, 41(2) 285-298.
582 Jex, C.N., Phipps, S.J., Baker, A, and Bradley, C. 2013. Reducing uncertainty in the climatic
583 interpretations of speleothem δ^{18}O. Geophysical Research Letters, 40, 2259–2264
584 Lachniet, M.S. 2009. Climatic and environmental controls on speleothem oxygen-isotope values.
585 Quaternary Science Reviews, 28, 412-432
586 Lis, G., Wassenaar, I.L. and Hendry, M.J., 2007. High-precision laser spectroscopy D/H and 18O/16O
587 measurements of microliter natural water samples. Analyt. Chem. 80,287-293
588 Mariethoz, G., Baker, A., Sivakumar, B., Hartland, A. and Graham, P. 2012. Chaos and irregularity in
589 karst percolation. Geophys. Res. Lett., L23305
590 Miller, G.H., Magee, J.W., and Jull, A.J.T., 1997. Low-latitude glacial cooling in the Southern
591 Hemisphere from amino-acid racemisation in emu eggshells. Nature 385, 241-244.

McDonald, J., Drysdale, R., Hill, D., Chisari, R. and Wong, H. 2007. The hydrochemical response of cave drip waters to sub-annual and inter-annual climate variability, Wombeyan Caves, SE Australia. Chemical Geology, 244, 605-623.

Nimmo, J. R. 2010. Theory for Source-Responsive and Free-Surface Film Modeling of Unsaturated Flow, Vadose Zone J., 9, 295–306, doi:10.2136/vzj2009.0085

Osborne R.A.L., 2007. Cathedral Cave, Wellington Caves, New South Wales, Australia. A multiphase, non-fluvial cave. Earth Surface Processes and Landforms, 32, 2075-2103.

Osborne, R.A.L., 2010. Rethinking eastern Australian caves. Geological Society, London, Special Publications, 346, 289-308.

Pape, J.R., Banner, J.L., Mack, L.E., Musgrove, M., and Guilfoyle, A., 2010, Controls on oxygen isotope variability in precipitation and cave drip waters, central Texas, USA: Journal of Hydrology, 385, 203-215.

Rutlidge, H., Baker, A., Marjo, C., Andersen, M.S., Graham, P.W., Cuthbert, M.O., Rau, G.C., Roshan, H., Markowska, M., Mariethoz, G. and Jex, C., submitted. Dripwater organic matter and trace element geochemistry in a semi-arid karst environment: implications for speleothem paleoclimatology. Geochimica et Cosmochimica Acta.

Sonntag, C., Christmann, D. and Munnich, K.O., 1985. Laboratory and field experiments on infiltration and evaporation of soil water by means of deuterium and oxygen-18. In: Proc. IAEA/GSF Meeting, Vienna, 1984, IAEA TECDOC 357: 145-159

Spötl, C., Fairchild, I.J., and Tooth, A.F., 2005. Cave air control on dripwater geochemistry, Obir caves (Austria): implications for speleothem deposition in dynamically ventilated caves. Geochimica et Cosmochimica Acta, 69, 2451-2468.

Treble, P.C., Bradley, C., Wood, A, Baker, A., Jex, C.N., Fairchild, I.J., Gagan, M.K., Cowley, J. and Azcurra, C., 2013. An isotopic and modelling study of flow paths and storage in Quaternary calcarenite, SW Australia: implications for speleothem paleoclimate records. Quaternary Science Reviews, 64, 90-103

618 Van Ommen, T.D. and Morgan, V., 2010. Snowfall increase in coastal East Antarctica linked with
619 southwest Western Australian drought. Nature Geoscience 3, 267-272.
620 Wassenaar, L.I., Hendry, M.J., Chostner, V.L. and Lis G.P. 2008. High Resolution Pore Water δ^2H and
621 $\delta^{18}O$ Measurements by H_2O(liquid)-H_2O(vapor) Equilibration, Environmental Science and Technology,
622 2008, 42 9262–9267
623

624 **Table captions**

625

626 Table 1. Drip water and local river and groundwater isotopic composition. For each drip site, a 'drip
627 water line' and its correlation coefficient is shown, along with the standard error of both gradient
628 (M) and intercept (C). Drip types are classified as soda straw stalactite (So), non soda-straw stalactite
629 (St) and non-soda-straw stalactite within flowstone (F)

630

631 Table 2. Parameter values estimated by manual calibration and used to generate model simulations
632 shown in Figure 3 & 7. Parameters not shown were subject to a Monte-Carlo analysis and have
633 ranges defined in Figure 7.

634

Figure captions

Figure 1. Cathedral Cave sampling locations. Boxes show the two monitoring sites: 1. the near-entrance site monitoring drip rate and 2. the deeper South Passage site monitoring drip rate and drip water isotopes. The locations of monitoring sites at the latter are shown in more detail in Figure 3c. Also labelled is 3: groundwater sample location 'The Well'. The cave survey is reproduced with permission of the Sydney University Speleological Society.

Figure 2. Schematic illustration of the modelled processes. Variables are all defined in the main text.

Figure 3. (a) Rainfall (grey line) and potential evaporation (black line); (b) modelled groundwater potential recharge; (c) drip rate for all Stalagmate drip loggers over the study period; (d) rainfall (dashed line) and drip water (solid line) monthly isotope samples.

Figure 4. (a) δ^2H vs δ^{18}O for monthly rainfall (closed circles) and infiltration (small closed squares). Local river water samples (open squares) and groundwater samples (open circles) are also presented. (b) Trend lines of the data presented in (a): Local Meteoric Water Line (dashed line) and δ^2H vs δ^{18}O regressions for each drip water site (solid lines). Regression equations and correlation coefficients are presented in Table 1. (b

Figure 5. Water δ^{18}O isotope time series shaded by slope of δ^2H vs δ^{18}O regression. >6.8, light grey dotted lines; 6.8-5.8, grey dot-dash lines; 5.8-4.8, dark grey dashed line; <4.8, black solid lines. Solid grey lines represent the periods of infiltration (Figure 2c).

Figure 6 Spatial distribution of Site 2 water isotope samples: see inset, Figure 1 for location within Cathedral Cave. Site ID and drip classification are as presented in Table 1. Shading and fill of the symbols shows the slope of δ^2H vs δ^{18}O regression as presented in Table 1.

Figure 7 (a) Results from Monte-Carlo modelling of drip water compositions shown against observations (solid lines, except dashed Site 319), and observed rainfall and modelled groundwater

potential recharge. Shaded area represents the isotopic distribution of the physically plausible model results (1927 out of 50 000). The model output for the most frequently used parameter values are highlighted (dots) and for no karst evaporation/fractionation (dot-dash) (b) Frequency distributions of the posterior parameter sets, normalised across the range of prior parameter values. Each parameter was free to vary between zero and the value defined in brackets. For example, m was free to vary randomly between 0 and -5 but most models that had a reasonable fit have values of around -0.2.

***Highlights (for review)**

1 Isotopic composition of cave drip waters in a semi-arid karst terrane are reported.

2 Their isotopic composition is heavier than the weighted mean annual precipitation.

3 Modelling confirms sub-surface evaporation affects drip water isotopic composition.

4 Relevant to the interpretation of speleothem records from arid and semi-arid regions.

5

Figure 1

Click here to download high resolution image

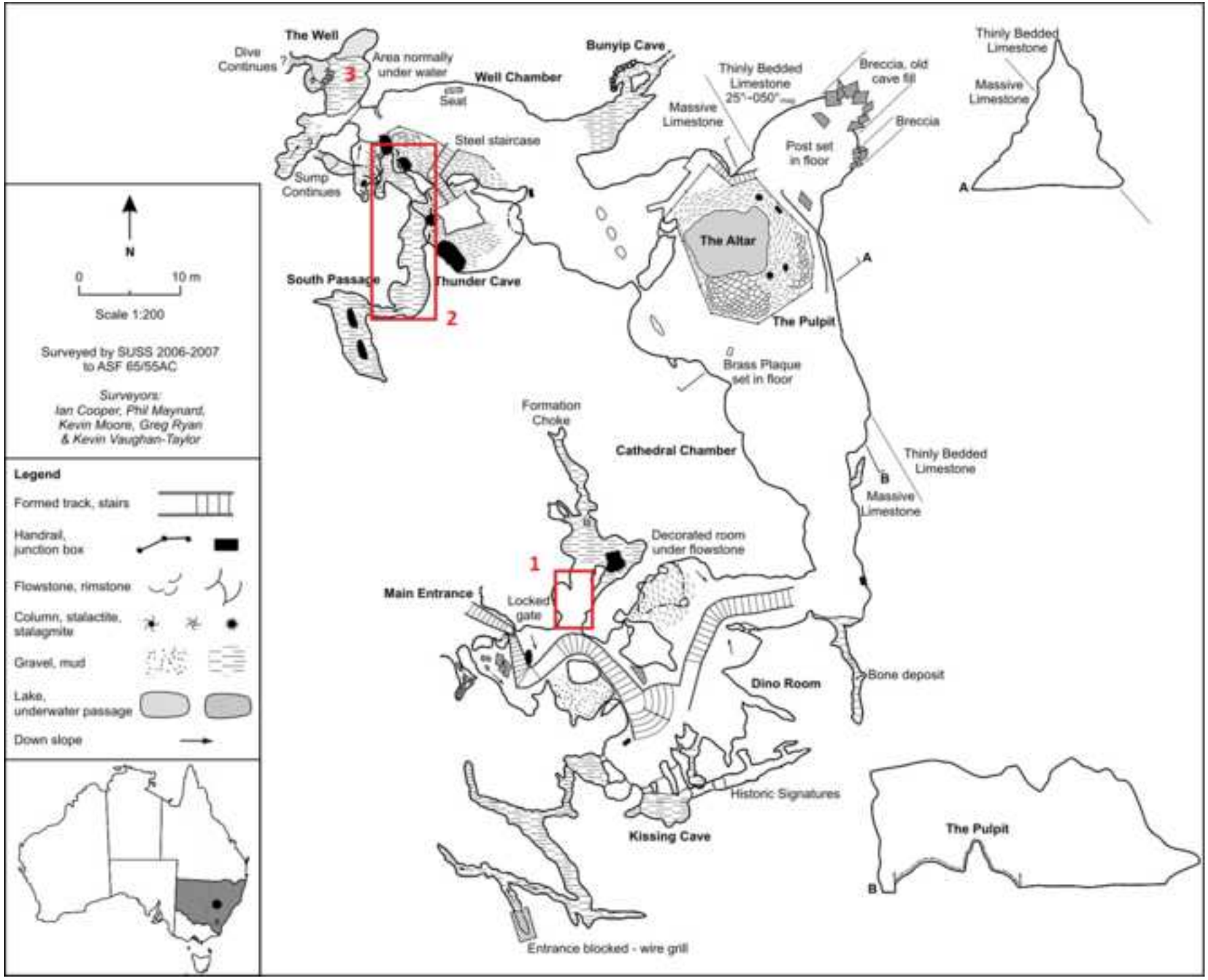

Figure 2

Click here to download high resolution image

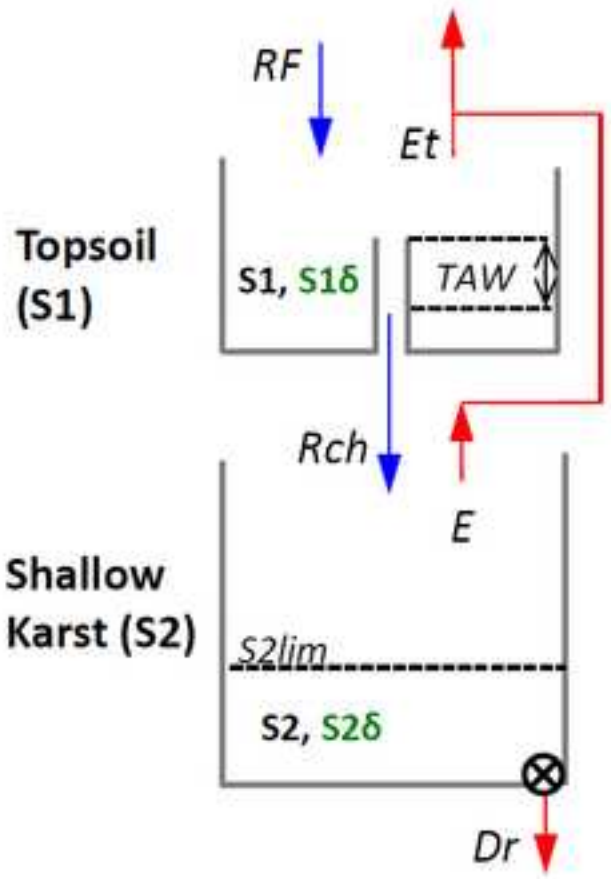

$$S1_{t+\Delta t} = S1_t + (RF_t - AE_t - Rch_t).\Delta t$$

$$S1\delta_{t+\Delta t} = (S1\delta_t.(S1_t - (AE_t + Rch_t).\Delta t) + RF\delta_t.RF_t\,\Delta t)/S1_{t+\Delta t}$$

$$S2_{t+\Delta t} = S2_t + (Rch_t - E - Dr_t).\Delta t \qquad Dr_t = \tau.S2_t$$

If $S2_t > S2lim$

Then $S2\delta_{t+\Delta t} = (S2\delta_t.(S2_t - (Dr_t + E).\Delta t) + S1\delta_t.Rch_t.\Delta t)/S2_{t+\Delta t}$

Else $S2\delta_{t+\Delta t} = (S2\delta_t - m).f^n + m$

Figure 3

Click here to download high resolution image

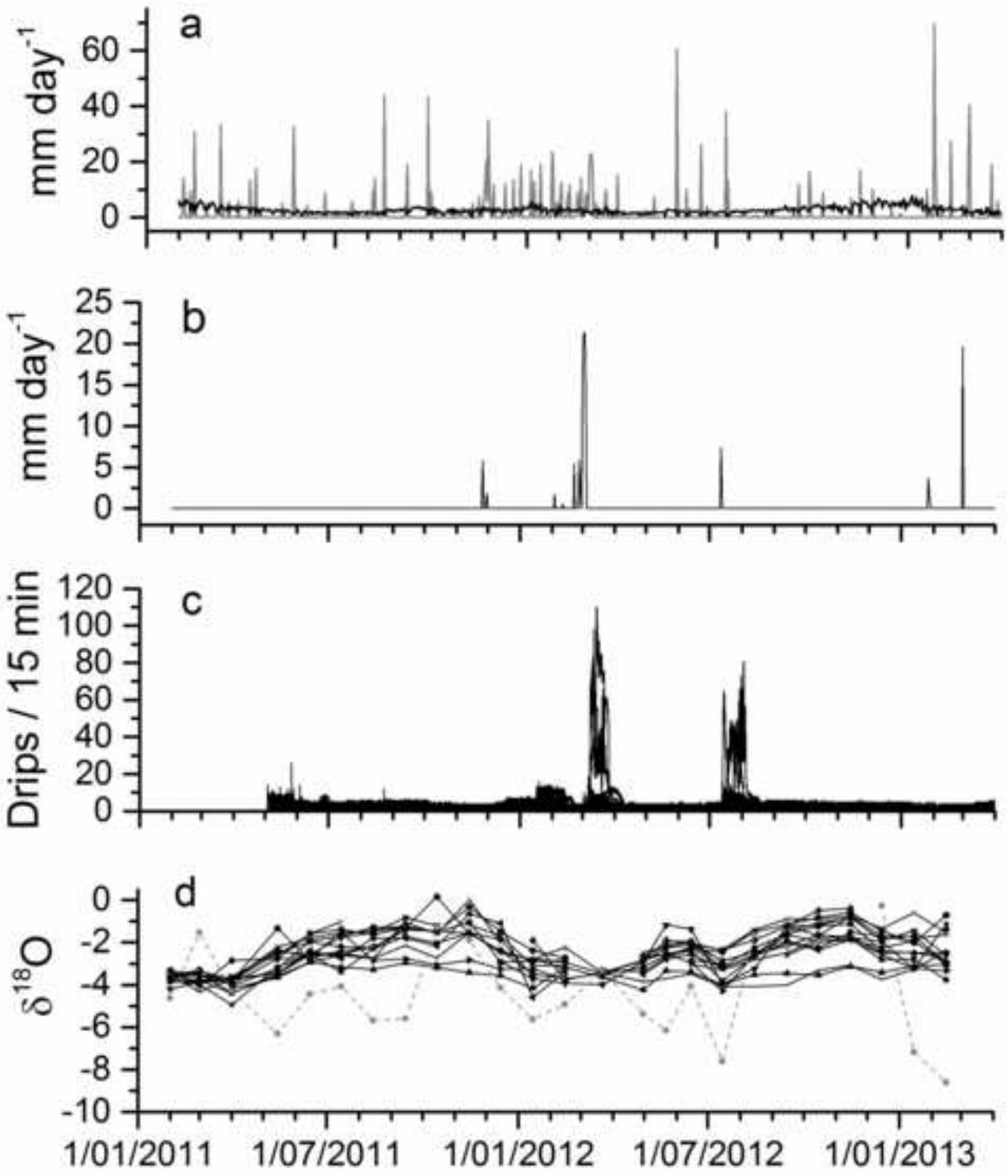

Figure 4

Click here to download high resolution image

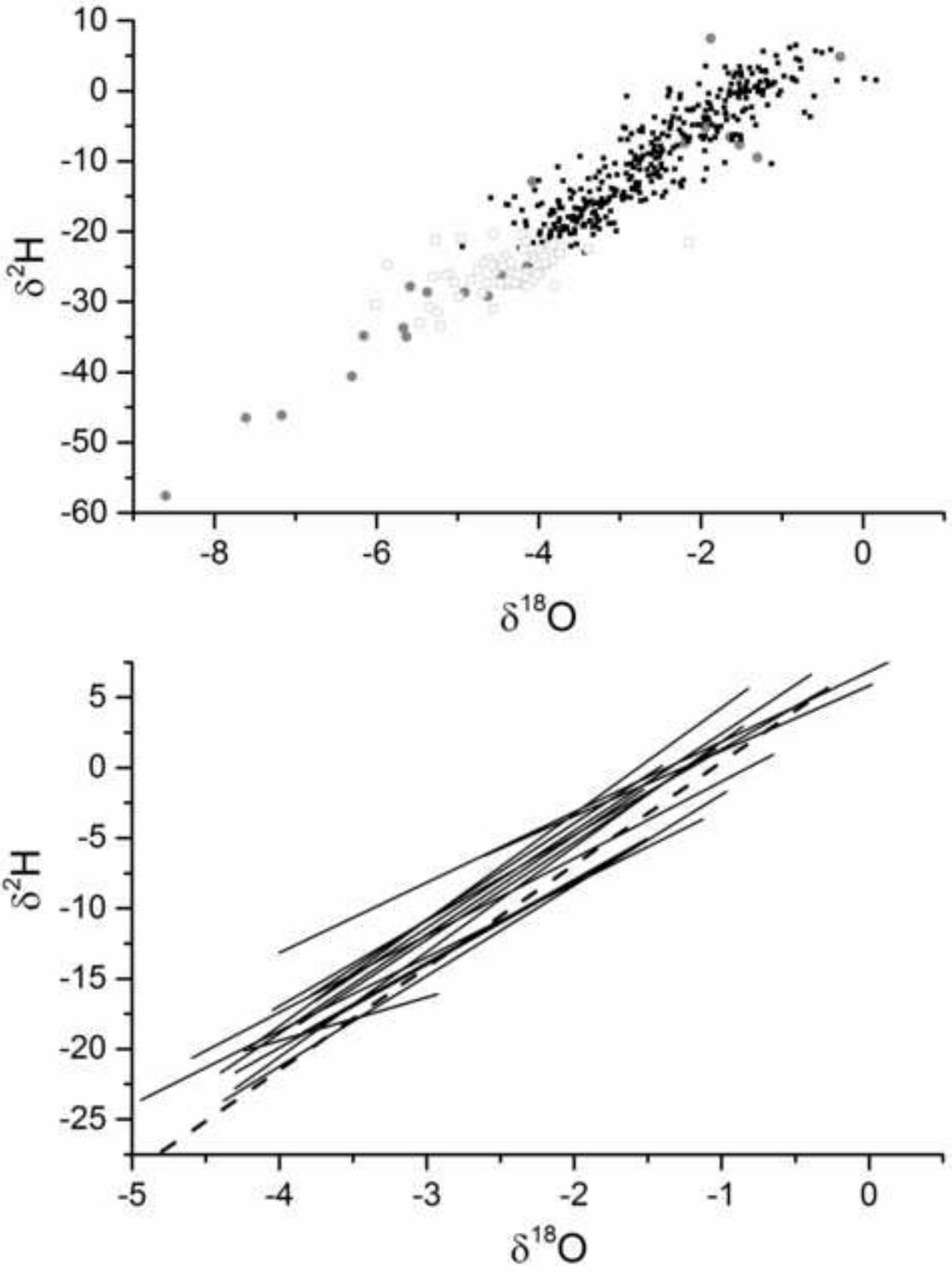

Figure 5

Click here to download high resolution image

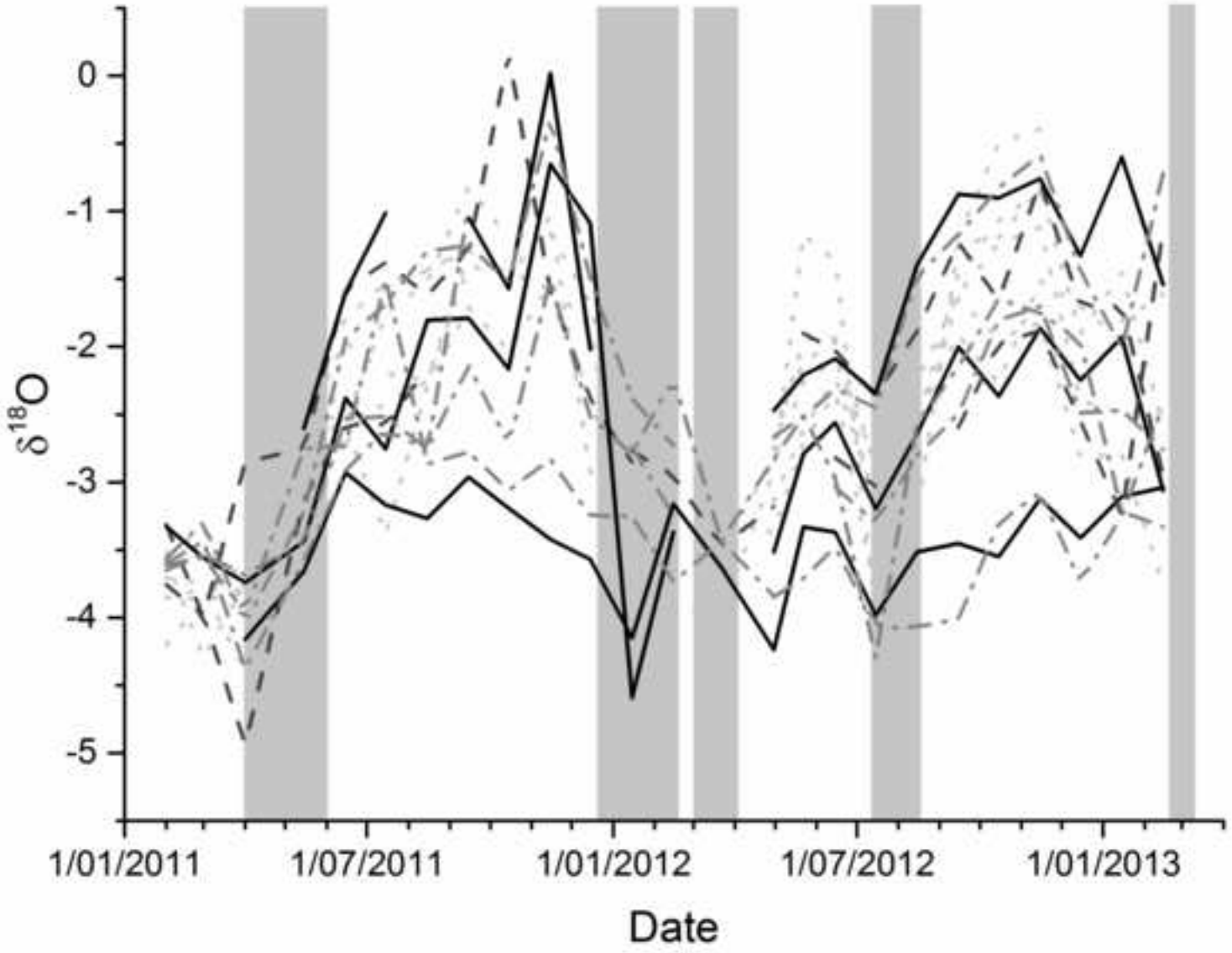

Figure 6

Click here to download high resolution image

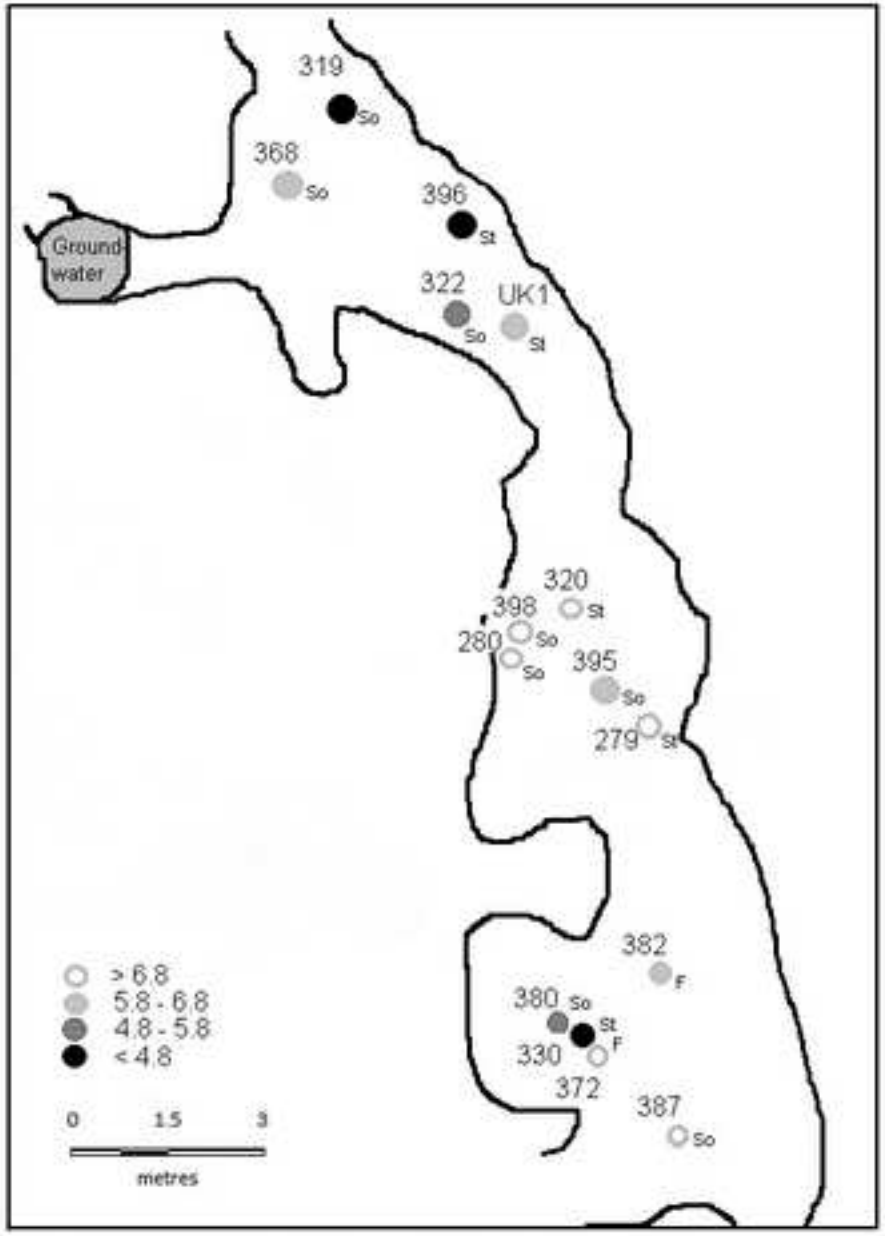

Figure 7a

Click here to download high resolution image

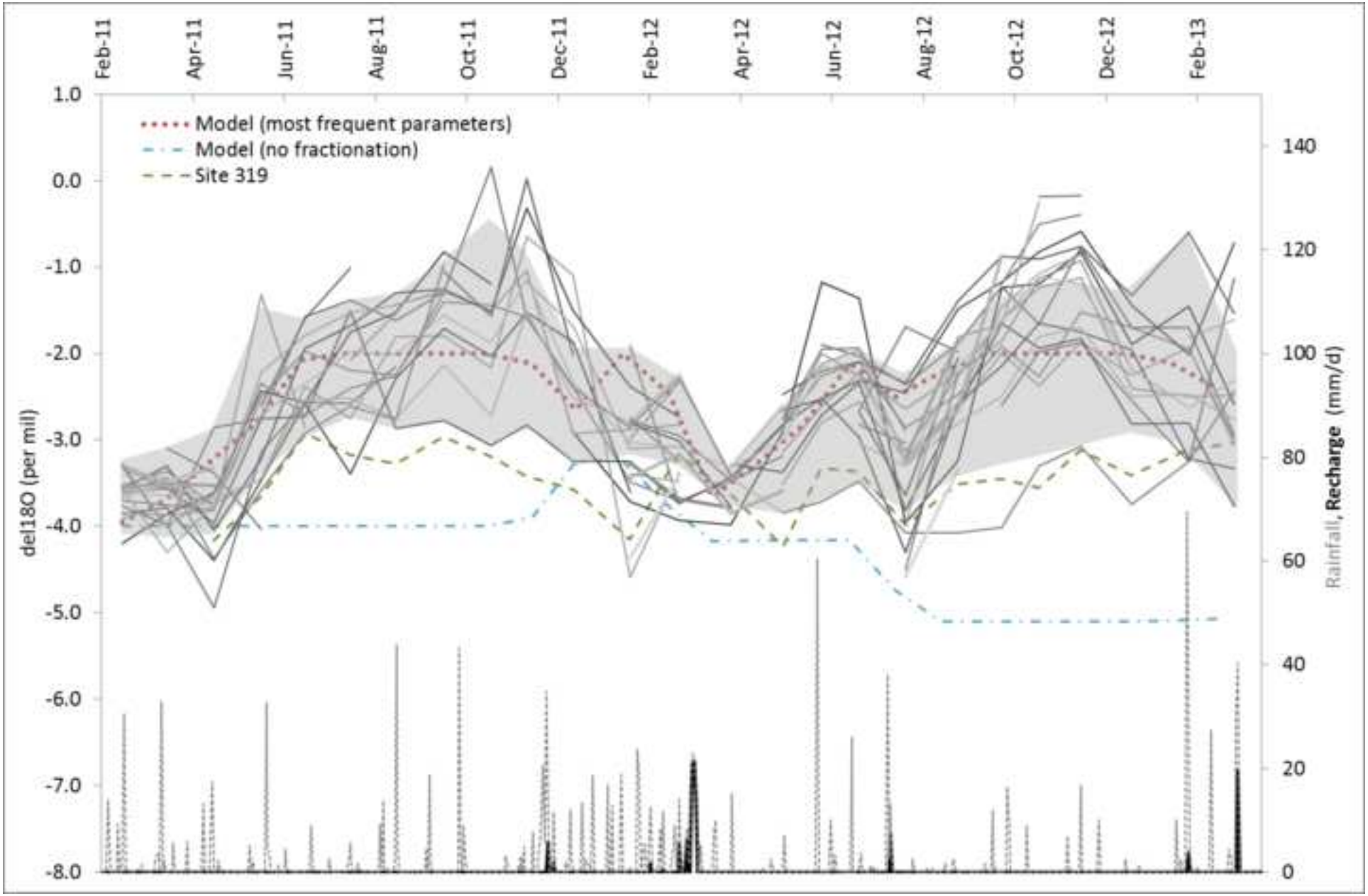

Figure 7b

Click here to download high resolution image

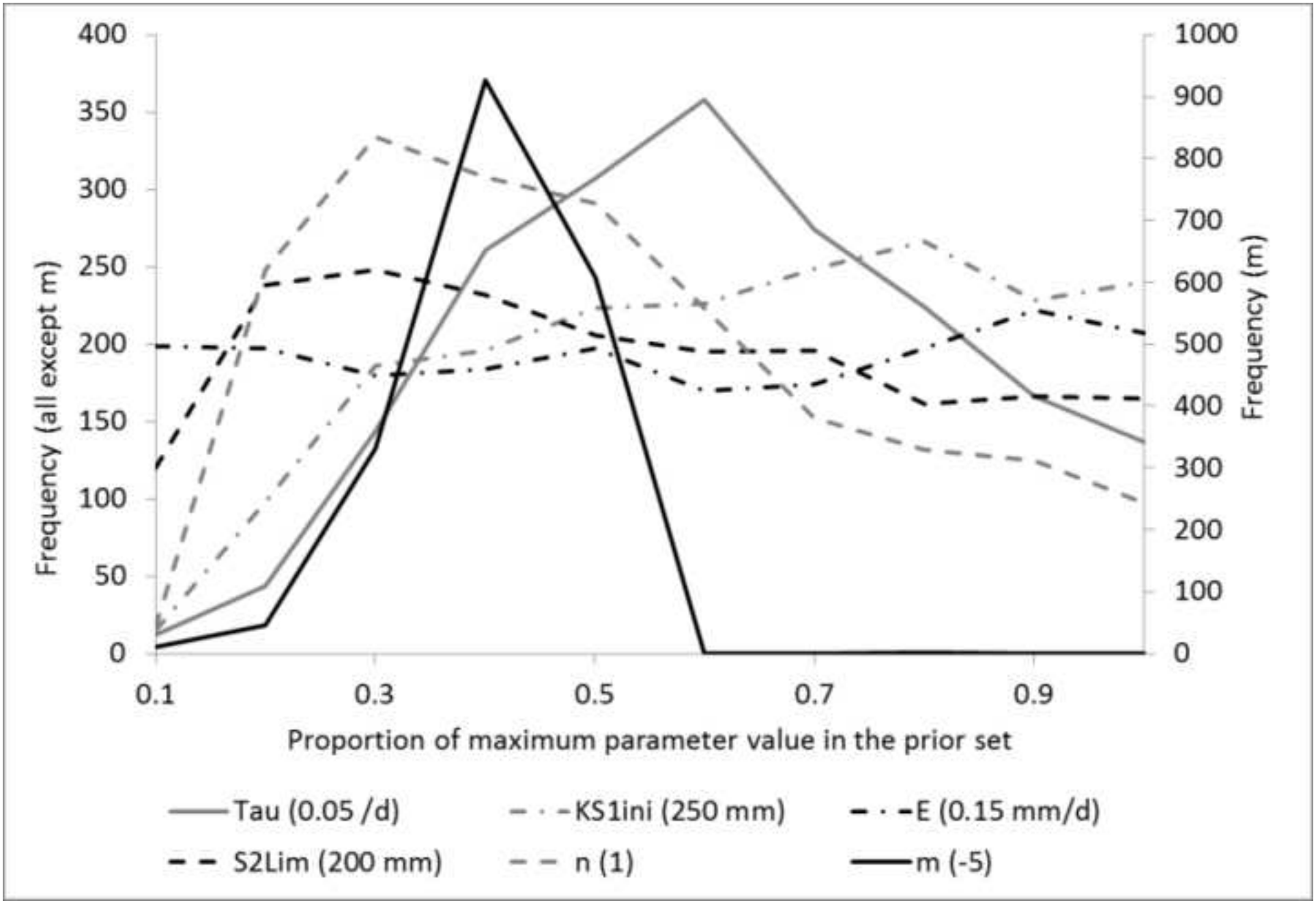

Table 1

Click here to download Table: Cuthbert et al_Table_1.docx

Table 1. Drip water and local river and groundwater isotopic composition. For each drip site, a 'drip water line' and its correlation coefficient is shown, along with the standard error of both gradient (M) and intercept (C). Drip types are classified as soda straw stalactite (So), non soda-straw stalactite (St) and non-soda-straw stalactite within flowstone (F)

Site ID	*Drip Type*	*Mean (drips/ 15min)*	*Median (drips/ 15 min)*	*Maximum (drips/ 15 min)*	*$\delta^{18}O$*		*$\delta^{2}H$*		*Number of samples*		*$\delta^{2}H = M * \delta^{18}O + C$*				
					mean	*sd*	*mean*	*sd*	*N*		*M*		*C*		*r*
279	St	8.28	1.00	368.00	-2.81	0.84	-10.52	6.75	24		7.03	0.81	9.22	2.38	0.88
280	So	0.89	1.00	3.00	-2.50	0.78	-7.38	6.18	25		6.85	0.82	9.76	2.13	0.87
319	So	1.85	2.00	14.00	-3.45	0.38	-17.72	1.99	23		3.08	0.92	-7.08	3.21	0.59
320	St	3.04	0.00	110.0	-2.43	1.16	-6.53	9.42	24		7.54	0.62	11.81	1.67	0.93
322	So	0.32	0.00	3.00	-1.98	0.91	-3.08	5.76	22		5.00	0.87	6.85	1.88	0.79
330	St	nd	nd	nd	-2.62	0.90	-9.84	6.10	24		4.49	0.86	5.47	2.36	0.81
368	So	nd	nd	nd	-2.90	0.71	-13.42	5.06	25		5.91	0.82	3.74	2.45	0.83
372	F	0.36	0.00	2.00	-2.36	0.90	-7.82	6.94	23		6.91	0.74	8.51	1.85	0.90
380	So	nd	nd	nd	-2.88	0.84	-12.85	5.34	19		5.23	0.88	2.24	2.63	0.82
382	F	nd	nd	nd	-1.96	0.98	-4.51	6.72	24		6.09	0.67	7.39	1.45	0.89
387	So	nd	nd	nd	-2.24	1.03	-6.13	7.70	18		6.90	0.73	9.33	1.80	0.92
395	So	3.90	3.00	11.00	-2.76	0.64	-12.43	4.79	24		5.90	0.99	3.84	2.79	0.79
396	St	nd	nd	nd	-1.51	0.73	-1.16	4.62	18		4.63	1.05	5.83	1.74	0.73
398	So	nd	nd	nd	-2.19	0.96	-7.06	7.63	22		7.47	0.63	9.33	1.49	0.94
UK1	St	nd	nd	nd	-3.30	0.75	-16.71	5.79	20		6.45	0.98	4.54	3.31	0.83
RAIN					-4.28	2.18	-23.54	16.48	24		7.29	0.43	7.68	2.08	0.96
Rivers															
MACQUARIE					-4.27	0.75	-24.58	3.06	18						
BELL					-4.45	0.59	-26.24	3.68	18						
Groundwater															
ANTICLINE					-4.43	0.53	-25.50	1.44	18						
WELL					-4.46	0.44	-26.41	2.34	18						

Table 2

Click here to download Table: Cuthbert et al_Table_2.docx

Parameter	***Description***	***Value***	***Units***
SMD_i	initial soil moisture deficit	TAW	mm
θ_{FC}	field capacity of soil	25	%
θ_{WP}	wilting point of soil	5	%
Z_e	soil depth subject to evaporative drying	0.1	m
Z_r	rooting depth	0.47	m
K_c	crop coefficient	1	-
p	RAW to TAW ratio	0.5	-
B	proportion of bare soil	0.1	-
$S1\delta_0$	Initial δ18O of soil store	-4	‰
$S2\delta_0$	Initial δ18O of karst store	-4	‰

Table 2. Parameter values estimated by manual calibration and used to generate model simulations shown in Figure 3 & 7. Parameters not shown were subject to a Monte-Carlo analysis and have ranges defined in Figure 7.

Supplementary table 1

Click here to download Supplementary material for on-line publication only: Cuthbert et al Supplemental Table 1 Rainfall Double

Supplementary table 2

Click here to download Supplementary material for on-line publication only: Cuthbert et al Supplementary Table 2 Drip rate data

Supplementary table 3

Click here to download Supplementary material for on-line publication only: Cuthbert et al Supplementary Table 3 Drip water an